Quantitative imaging of flux vortices in the type-II superconductor MgB$_2$ using cryo-Lorentz transmission electron microscopy

M. J. G. Cottet,[1] M. Cantoni,[2] B. Mansart,[1] D. T. L. Alexander,[2] C. Hébert,[2] N. D. Zhigadlo,[3] J. Karpinski,[3,4] and F. Carbone[1]

[1]*Laboratory for Ultrafast Microscopy and Electron Scattering, ICMP, Ecole Polytechnique Fédérale de Lausanne, CH-1015 Lausanne, Switzerland*

[2]*Centre Interdisciplinaire de Microscopie Electronique, CIME, Ecole Polytechnique Fédérale de Lausanne, CH-1015 Lausanne, Switzerland*

[3]*Laboratory of Solid State Physics, ETH Zurich, CH-8057 Zurich, Switzerland*

[4]*Laboratory of Nanostructures and Novel Electronic Materials, ICMP, Ecole Polytechnique Fédérale de Lausanne, CH-1015 Lausanne, Switzerland*

Imaging of flux vortices in high quality MgB$_2$ single crystals has been successfully performed in a commercial field-emission gun-based transmission electron microscope. In cryo-Lorentz microscopy, the sample quality and the vortex lattice can be monitored simultaneously, allowing one to relate microscopically the surface quality and the vortex dynamics. Such a vortex motion ultimately determines the flow resistivity ρ_f, the knowledge of which is indispensable for practical applications such as superconducting magnets or wires for magnetic resonance imaging. The observed patterns have been analyzed and compared with other studies by cryo-Lorentz microscopy or Bitter decoration. We find that the vortex lattice arrangement depends strongly on the surface quality obtained during the specimen preparation, and tends to form a hexagonal Abrikosov lattice at a relatively low magnetic field. Stripes or gossamerlike patterns, recently suggested as potential signatures of an unconventional behavior of MgB$_2$, were not observed.

In superconductors, identifying the relationship between the transverse force felt by the triangular array of vortices in response to a transport current and the pinning force resulting from defects or inhomogeneities is of capital importance. This is because flux motion induces a longitudinal resistive voltage, which is a source of energy dissipation and ultimately hinders a material's performance in applications.[1] Indeed, in type-II superconductors, the superconducting state is not completely destroyed when an external magnetic field exceeds the lower critical one, H_{c1}. The external field partially penetrates into the material in the form of midget microscopic filaments called vortices. As a first approximation (Bardeen-Stephen model[2]), the core of each vortex, where superconductivity is suppressed, is modeled by a cylinder with a radius given by the coherence length ξ, and is surrounded by circling supercurrents over a distance corresponding to the London penetration depth λ. It is assumed that the core of each vortex is a conventional metallic state inside of which the energy dissipation is dominated by impurity scattering.[3] Each vortex carries a magnetic flux equal to $\Phi_0 = h/(2e)$, where h is the Planck constant and e is the elementary charge.[4] Due to their mutual repulsion, in a defect-free superconductor, vortices tend to form a two-dimensional (2D) close-packed triangular array surrounded by a hexagonal pattern of other vortices, called the Abrikosov lattice.[5] Cryo-Lorentz Transmission Electron Microscopy (cryo-LTEM) allows the direct observation of quantized flux lines and so is a key technique for understanding the flux flow resistivity associated with the viscous motion of the vortices.[6] It is with the out-of-focus imaging of the Lorentz mode that individual flux quanta can be imaged, as well as superconducting or magnetic domains (Fig. 1, Fresnel mode).[7] Specifically, flux lines can be imaged thanks to the deflection imparted to the electrons by the magnetic flux associated with each vortex. In this paper, we investigate the formation and the dynamics of flux vortices in MgB$_2$ single crystals using cryo-LTEM with a defocus of ≈ 15 mm.[8]

MgB$_2$ is a type-II superconductor with $T_c = 39$ K. It crystallizes in a hexagonal structure consisting of alternating honeycomb layers of B and hexagonal layers of Mg atoms, with $a = b = 3.1432 \pm 0.0315$Å and $c = 3.5193 \pm 0.0323$ Å.[9] In the low-field limit, the coherence length in the ab plane has been found as $\xi_{ab} = 5.5$ nm,[10] and λ_{ab} lies between 110 and 130 nm (Ref. [11]) [$\xi_c = 51$ nm and $\lambda_c = 33.6$ nm (Ref. [12])]. The lower critical field H_{c1} in the c direction is around 250 mT and the upper critical field H_{c2} is lower than 3 T at 5 K.[13] MgB$_2$ is a two-band system with two different gap amplitudes: $\Delta_\sigma = 7.1 \pm 0.1$ meV following a BCS-like temperature dependence, and $\Delta_\pi = 2.80 \pm 0.05$ meV showing deviations at $T \geqslant 25$ K as shown by Gonnelli *et al.*[14]

Recently, Gurevich *et al.*[15] have demonstrated the tunability of H_{c2} for different MgB$_2$ samples when alloyed with nonmagnetic impurities; H_{c2} values well above those of some competitive noncuprate superconductors were obtained, thereby increasing the potential applications of this compound. According to the value of the Ginzburg-Landau parameter in the ab-plane reported by Caplin *et al.* ($\kappa \cong 4$ at 5 K), this material is far into the limit of type-II superconductors.[13] However, this classification has recently been questioned by the proposition of a novel superconducting state between type I and type II which could stabilize in an unconventional vortex pattern formed by stripes and gossamerlike shapes (vortex clusters emerging at low magnetic field). The observation of such a vortex pattern has been reported by Moshchalkov *et al.*[12] and Nishio *et al.*[16] at very low fields, while, more recently, cryo-LTEM experiments have instead shown a distorted square lattice arrangement surrounded by vortex lines resulting from the specimen preparation,[17] different from a conventional and stable triangular pattern.[18–20]
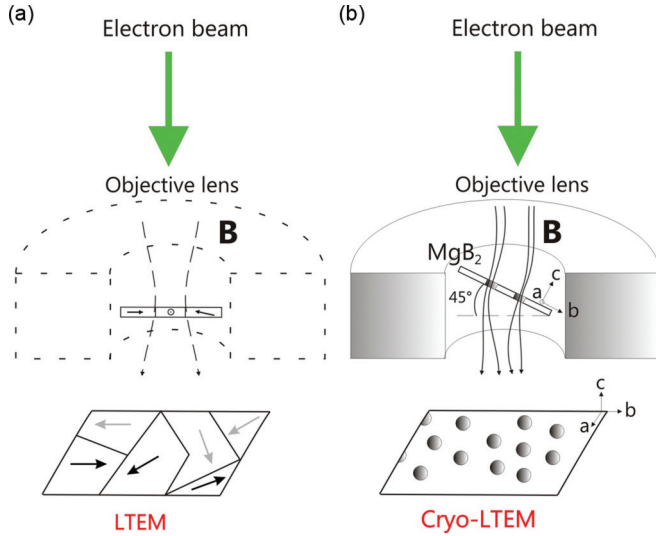
FIG. 1. (Color online) Lorentz microscopy or phase contrast microscopy. (a) Example of Lorentz Transmisson Electron Microscopy (LTEM) on a magnetic compound; there is a small residual magnetic field near the specimen, the objective lens is off. (b) Cryo-Lorentz transmission electron microscopy on a superconductor (cryo-LTEM); the objective lens is weakly activated to induce a magnetic field near the specimen. The electrons are deflected by the magnetic fields of the vortices giving rise to black and white features as shown on the image plane.

In this paper, we perform new cryo-LTEM experiments on MgB_2 and confirm that its distribution of flux quanta follows a conventional type-II behavior. Vortices tend to form a stable triangular pattern at relatively low magnetic fields due to the symmetrical surrounding resulting from short-range repulsion.[21] Stripes or gossamerlike patterns are not observed, although distortions of the expected triangular arrangement are visible close to the sample edge. This suggests that the presence of such other patterns probably results from a nonideal surface obtained during the sample preparation process, and does not necessarily justify the assignment of an unconventional class of superconductors by means of surface sensitive techniques such as Bitter decoration.[12,16] In fact, to be in equilibrium in a certain position, the vortex lines must have a total superfluid velocity equal to zero. This can be accomplished if each vortex of the pattern is surrounded by a symmetrical array like a triangular or a square pattern. However, the square array exhibits only an unstable equilibrium since small displacements tend to be spontaneously generated; the triangular lattice instead has the lowest free energy. This is confirmed by the solution of the Ginzburg-Landau equations of the Abrikosov type for a defect-free type-II superconductor for magnetic fields below H_{c2}, giving the value of the parameter determining the most favorable configuration of all periodic solutions for both patterns, β_A ($\beta_A = \langle \Psi_L^4 \rangle / \langle \Psi_L^2 \rangle^2$, $\beta_A^{tri} = 1.16$, and $\beta_A^{sq} = 1.18$), where $\langle \Psi_L \rangle$ is a general solution to the linearized Ginzburg-Landau equation.[5,20] Moreover, pinning results from spatial inhomogeneity since local variations of ξ, λ, or H_c leads to a local change of the free energy per unit of vortex line, causing some vortices to be preferentially located at certain positions. To be relevant, the material defects must stay in the
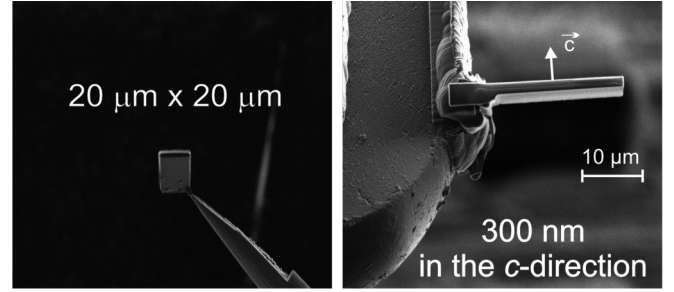

FIG. 2. Images of the specimen during the preparation process. The sample is pretilted at $45°$ when attached to a dedicated TEM grid; the sample is electron transparent in the c direction.

order of 10^{-6}–10^{-5} cm, in order to avoid electronic scattering which limits the mean free path l.[22]

MgB_2 single crystals were synthesised via the decomposition of $MgNB_9$, as described in Ref. 23. To be electron transparent, the specimen was prepared using a Zeiss NVision 40 Focused Ion Beam (FIB): the sample was thinned to 300 nm in the c direction, and pretilted at $45°$ when attached on a TEM grid (as shown in Fig. 2). A Gatan single tilt helium cooling holder was used to cool the specimen down to 5 K, and the images were acquired digitally on a Gatan 2k × 2k charge-coupled device camera mounted on a JEOL 2200FS TEM instrument using a field-emission gun operated at 200 keV.

In Fig. 3, a sequence of images showing flux vortices taken at 5 K and for different induced magnetic fields (specified on each image) is presented. The intensity of the field has been calculated via the density of vortices averaged across the region of interest. The images are tilt-compensated to correct for the apparent compression of the vortices in one direction due to the sample's configuration required to carry out cryo-LTEM [Fig. 1(B)]. The sequence begins at 50.8 G and the magnetic field is slowly increased to reach 188.7 G, where individual quanta cannot be distinguished anymore. When the temperature is increased above the superconducting transition temperature ($T = 65$ K) at a fixed magnetic field, no vortices are observed, as shown in the top right panel of Fig. 3. At low field, vortices are formed at the edge of the specimen,[24] and when the magnetic flux further penetrates an ideal type-II superconductor, the force density on the vortices α resulting from the Lorentz force tends to make them move,[22]

$$\alpha = J_{ext} \times \frac{B}{c} = (curl H) \times \frac{B}{4\pi}, \quad (1)$$

where J_{ext} represents the externally imposed currents, leaving out the equilibrium contribution coming from the response of the specimen.

The dark bands (or areas) present in each image are called bend contours and are due to diffraction contrast. To confirm this origin of such dark bands, it was checked that they vary in size and position when tilting the sample or changing the induced magnetic field (due to the imaging condition), as shown by the red dashed rectangles of Fig. 3 located at the same position (the origin of bend contours is shown in the bottom-right panel of Fig. 3).[25] As discussed later, flux vortices have poor contrast within these bend contours, impeding their analysis.
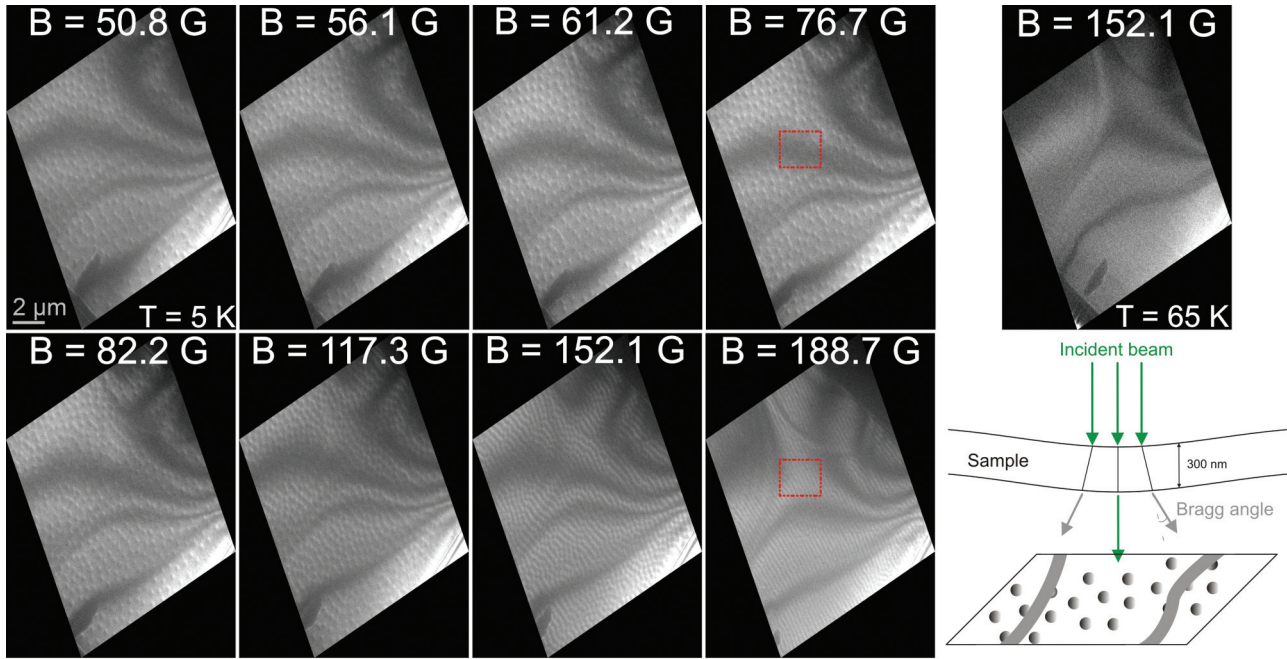
FIG. 3. (Color online) Series of tilt-compensated images showing flux vortices in MgB_2 taken at different magnetic fields (indicated on the images) and at a temperature of 5 K. The specimen is pretilted at $45°$ ($\pm 1°$). The scheme at the bottom right shows the origin of the bend contours. When the sample is locally curved the incident beam is not parallel to the *hkl* plane; the Bragg condition is then fulfilled resulting in dark bands in the obtained image. The dashed rectangles show how bend contours move as a function of the induced magnetic field (temperature or small tilt difference).

To obtain a quantitative information related to the vortex network, we calculate the sixfold bond-orientational order parameter $|\Psi_6|$. This parameter measures the instantaneous crystalline orientation between vortices separated by a distance r_{ij} and an angle θ_{ij} with two of its direct neighbors n_i. $|\Psi_6| = 1$ for a perfect Abrikosov lattice,[26]

$$\Psi_6(r_{ij},t) = \frac{1}{n_i} \sum_{j=0}^{n_i} \exp(6i\theta_{ij}). \quad (2)$$

This parameter was calculated by using a distribution map of the vortices obtained via a triangulation algorithm, which is a useful tool for efficiently solving many topography problems.[27] The Fiji open-source platform was used to carry out this triangulation, enabling fast image processing.[28] The locating of vortices is accomplished by determining the local maxima in an image and creating a binary image of the same size. An example is shown in Fig. 4(a). The Delaunay triangulation minimizes the maximum possible circumcircle for all triangles joining a given set of points, and it maximizes the minimum angle of those triangles [Fig. 4(b)].[29]

If the sample is divided into three areas separated by the bend contours (position taken at low field, below 120 G; see Fig. 3), the local value of $|\Psi_6|$ can be calculated to assess the homogeneity of the magnetic field in the sample related to the surface quality: these three areas are considered as defect free; the small portion of the sample close to the edge was not analyzed due to the presence of pinned vortices and distorted patterns. An example of this procedure is given in Fig. 4 where the vortex lattice in the different areas at the same magnetic field is displayed together with the corresponding Delaunay triangulation. In these areas, values of $|\Psi_6|$ equal to 0.29, 0.46,
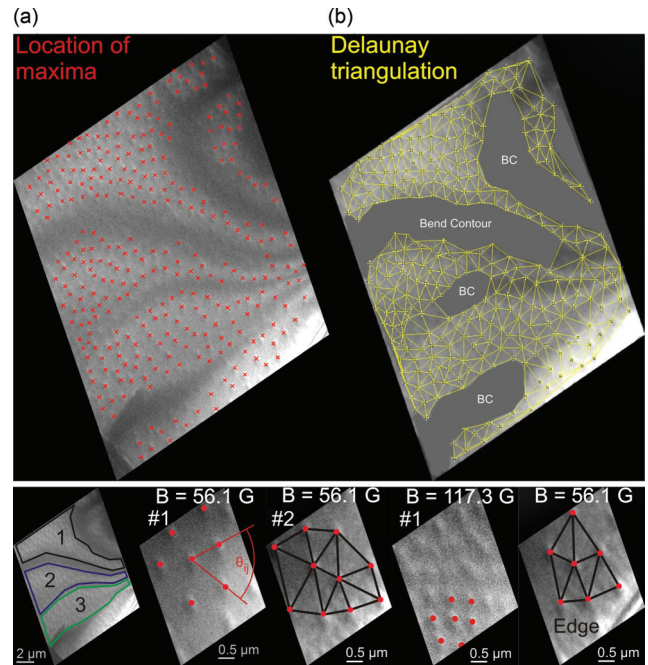

FIG. 4. (Color online) (a) Location of vortices (point location step); each red cross represents a maximum. Image taken at $T = 5$ K and $B = 56.1$ G. (b) Delaunay triangulation for the set of points determined in (a), each vortex is connected to its direct neighbors. The grey areas represent the bend contours (excluded for the triangulation). The bottom images (higher magnification, $4\times$) show examples of Delaunay triangulation of triangular arrays of vortex patterns for different induced magnetic fields (56.1 and 117.3 G) and different areas located between the bend contours; the bottom-right image shows a distorted pattern close to the sample edge.
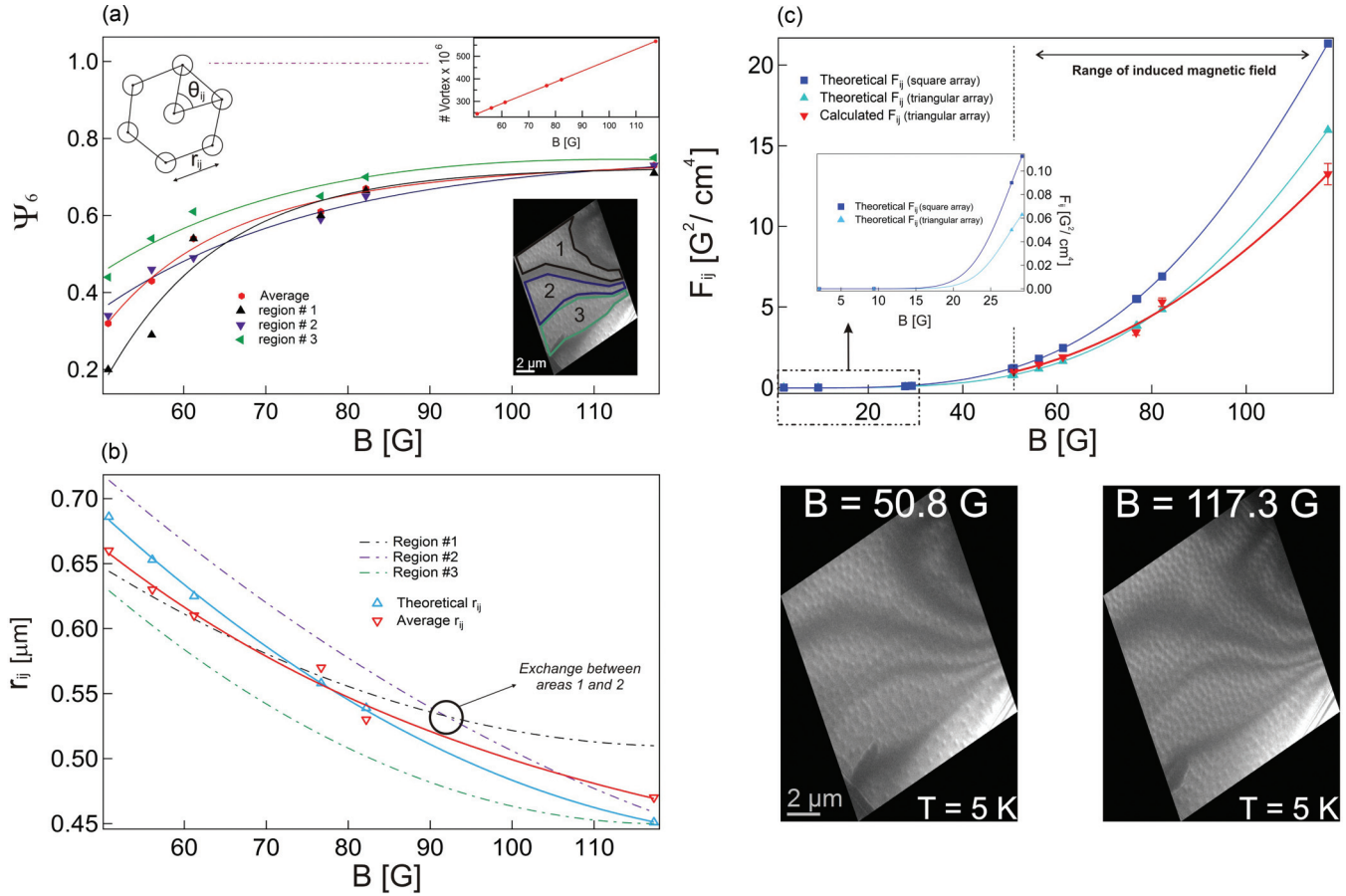
FIG. 5. (Color online) (a) Evolution of the sixfold parameter $|\Psi_6|$ as a function of the induced magnetic field B; $|\Psi_6| = 1$ (dashed line) represents a perfect triangular array of vortices. The inset upper-right graphic shows the evolution of the vortex density. (b) Evolution of the average distance between vortices r_{ij} as a function of B for the three regions. (c) Evolution of the interaction energy F_{ij} for a pair of vortices in the low flux density regime calculated from our data; the blue and the red curves represent respectively the theoretical evolution of F_{ij} for a square and a triangular array of vortices; the inset graph shows the evolution of F_{ij} at very low fields for the same patterns.

and 0.54 are found (average value corresponding respectively to the area labeled 1, 2, and 3). The same analysis was carried out throughout the specimen and for different magnetic fields obtaining a rather homogeneous distribution of $|\Psi_6|$ values; the vortices are not analyzed in the dark areas of the bend contours because the signal-to-noise ratio does not allow the accurate determination of their locations. In Fig. 5, the sixfold parameter, the distance between vortices and the interaction energy F_{ij}, are all displayed for the three areas of the sample. In the low flux density regime ($\Phi_0/B \gg \lambda^2$), F_{ij} is given by

$$\sum_{i>j} F_{ij} = \left(\frac{B}{\Phi_0}\right) \frac{z}{2} \frac{\Phi_0^2}{8\pi^2 \lambda_{ab}^2} K_0 \left(\frac{r_{ij}}{\lambda_{ab}}\right), \quad (3)$$

$$\sum_{i>j} F_{ij} \approx \frac{B z \Phi_0}{16\pi^2 \lambda_{ab}^2} \left(\frac{\pi \lambda_{ab}}{2a}\right)^{1/2} e^{-r_{ij}/\lambda_{ab}}, \quad (4)$$

where z represents the number of neighbors ($z = 6$ for a triangular array and $z = 4$ for a square pattern); the theoretical values were obtained using $r_{ij} = d(\Phi_0/B)$, with $d = 1.075$ for the triangular array and $d = 1$ for the square one.[22] All contributions except those coming from the nearest neighbors are neglected. According to the exponential term, for low magnetic fields, the triangular array will be lower

in energy than the square pattern. The derivative of F_{ij} with respect to B shows that the system undergoes a second-order phase transition at H_{c1}, where the induced magnetic field is continuous. In other words, there is a certain range of induced magnetic fields for which only one vortex will be formed until B becomes large enough to generate vortices separated by a distance $\approx \lambda$ for relatively high κ systems ($\xi_{ab} = 5.5$ nm and $\lambda_{ab} \cong 120$ nm), while B is discontinuous at H_{c1} for low κ systems.[30]

A similar trend is observed in these three regions: upon increasing magnetic field, the vortex density increases and the sixfold parameter tends to approach the Abrikosov value, even though our range of analyzed magnetic field does not allow the visualization of a perfect undistorted triangular array of vortices (to reach higher $|\Psi_6|$ values, higher spatial resolution in cryo-LTEM is needed in order to analyze the images taken at higher magnetic fields). The trend of F_{ij} [Fig. 5(c)] clearly confirms the stability of the triangular pattern over the square one for this regime, in which small displacements tend to grow. When the supercurrent starts to flow the vortices start to move under the Lorentz force if they are not pinned by the so-called "pinning centers." In this experiment, the force redistributing vortices within the specimen is enough to have

no vortex pinning (except at the edge), confirming the high quality of the sample surface and the close relation between the sample preparation and the observed behavior. In fact, when the pinning is weak with respect to the driving force, vortices will start to move in a steady motion with a velocity related to the viscous damping of the material, without jumping from one pinning site to another. This regime is called flux flow.[31] The calculation of the sixfold parameter, as well as the average distance between vortices, reveals two different behaviors depending on the region considered. Indeed, region 3 is close to the edge of the sample, leading to a larger density of vortices at low field, since they enter by the edge of the specimen and then are pushed towards the middle of the sample.[24] The high value of $|\Psi_6|$ at low B, as well as the shortest distance between vortices, confirm this trend. On the other hand, close to the edge, inhomogeneities are enhanced and deeply affect the movement of the vortices and the arrangements they adopt leading to the flux creep regime in this small portion of the sample (visible at the bottom of region 3). An example of a distorted vortex network at the edge is shown in the bottom right panel of Fig. 4. When the magnetic field increases, vortices tend to form an Abrikosov lattice in the rest of the specimen, as shown for $B = 188.7$ G (Fig. 3), where due to a slightly different specimen orientation (small tilt) the bend contours are shifted and the geometry of the vortex network is revealed. At 117.3 G, the average value of $|\Psi_6| = 0.73$, and reaches 0.91 locally (representing around 1/3 of the analyzed region). The theoretical calculation of the average distance for a triangular array [Fig. 5(b)] is in good agreement with

the experiments, so validating our calculated magnetic fields. Moreover, the crossing of the dashed curves in the same graph shows that vortices move from one region to another, confirming that bend contours are only related to diffraction contrast and do not affect the geometry of the vortex lattice.

In conclusion, the authors report the imaging of flux vortices in MgB_2 single crystals using cryo-LTEM. Transmission electron microscopy has the advantage of being sensitive to the magnetic field throughout the thickness of the sample and not only at the surface. The vortex lattices exhibit the behavior predicted by the theory.[5] No stripes or gossamerlike patterns were observed. Rather, their arrangement tends to that of the hexagonal Abrikosov lattice confirming that MgB_2 is a prototypical type-II superconductor. This finding is related to the high surface quality obtained during the sample preparation by focused ion beam that allows the direct observation of the vortex dynamics in a defect-free specimen. If the trend of $|\Psi_6|$ is to be verified for larger values of B (around 200 G and above) spatial resolution will need to be improved in order to distinguish individual quanta at these high fields. We conclude that the small distortion of the triangular lattice, even if our range of B is far away from H_{c2}, is related to impurities coming from the growing process itself, since the surface obtained after the preparation step is defect-free.

[1] Y. Matsuda, A. Shibata, K. Izawa, H. Ikuta, M. Hasegawa, and Y. Kato, Phys. Rev. B **66**, 014527 (2002).

[2] J. Bardeen and M. J. Stephen, Phys. Rev. **140**, A1197 (1965).

[3] Y. B. Kim and M. J. Stephen, in *Superconductivity*, edited by R. D. Parks (Marcel Dekker, New York, 1969), p. 1107.

[4] B. S. Deaver and W. M. Fairbank, Phys. Rev. Lett. **7**, 43 (1961).

[5] A. A. Abrikosov, Sov. Phys. JETP **5**, 1174 (1957).

[6] A. Shibata, M. Matsumoto, K. Izawa, Y. Matsuda, S. Lee, and S. Tajima, Phys. Rev. B **68**, 060501 (2003).

[7] K. Harada, T. Matsuda, J. Bonevich, M. Igarashi, S. Kondo, G. Pozzi, U. Kawabe, and A. Tonomura, Nature (London) **360**, 51 (1992).

[8] J. N. Chapman, E. M. Waddell, P. E. Batson, and R. P. Ferrier, Ultramicroscopy **4**, 283 (1979).

[9] S. L. Bud'ko, G. Lapertot, C. Petrovic, C. E. Cunningham, N. Anderson, and P. C. Canfield, Phys. Rev. Lett. **86**, 1877 (2001).

[10] J. C. Loudon, C. J. Bowell, N. D. Zhigadlo, J. Karpinski, and P. A. Midgley, Phys. Rev. B **87**, 144515 (2013).

[11] F. Manzano, A. Carrington, N. E. Hussey, S. Lee, A. Yamamoto, and S. Tajima, Phys. Rev. Lett. **88**, 047002 (2013).

[12] V. Moshchalkov, M. Menghini, T. Nishio, Q. H. Chen, A. V. Silhanek, V. H. Dao, L. F. Chibotaru, N. D. Zhigadlo, and J. Karpinski, Phys. Rev. Lett. **102**, 117001 (2009).

[13] D. Caplin, Y. Bugoslavsky, L. F. Cohen, L. Cowey, J. Driscoll, J. Moore, and G. K. Perkins, Supercond. Sci. Technol. **16**, 176 (2003).

[14] R. S. Gonnelli, D. Daghero, G. A. Ummarino, V. A. Stepanov, J. Jun, S. M. Kazakov, and J. Karpinski, Phys. Rev. Lett. **89**, 247004 (2002).

[15] A. Gurevich, S. Patnaik, V. Braccini, K. H. Kim, C. Mielke, X. Song, L. D. Cooley, S. D. Bu, D. M. Kim, J. H. Choi, L. J. Belenky, J. Giencke, M. K. Lee, W. Tian, X. Q. Pan, A. Siri, E. E. Hellstrom, C. B. Eom, and D. C. Larbalestier, Supercond. Sci. Technol. **17**, 278 (2004).

[16] T. Nishio, V. H. Dao, Q. Chen, L. F. Chibotaru, K. Kadowaki, and V. V. Moshchalkov, Phys. Rev. B **81**, 020506 (2010).

[17] J. C. Loudon, C. J. Bowell, N. D. Zhigadlo, J. Karpinski, and P. A. Midgley, Physica C **474**, 18 (2012).

[18] M. R. Eskildsen, M. Kugler, G. Levy, S. Tanaka, J. Jun, S. M. Kazakov, J. Karpinski, and Ø. Fischer, Physica C: Superconductivity **388**, 143 (2003).

[19] D. Cribier, B. Jacrot, L. Madhav Rao, and B. Farnoux, Phys. Lett. **9**, 106 (1964).

[20] W. H. Kleiner, L. M. Roth, and S. H. Autler, Phys. Rev. **133**, A1226 (1964).

[21] A. L. Fetter, P. C. Hohenberg, and P. Pincus, Phys. Rev. **147**, 140 (1966).

[22] M. Tinkham, *Introduction to Superconductivity*, 2nd ed. (Dover, Mineola, NY, 1975).

[23] J. Karpinski, S. M. Kazakov, J. Jun, M. Angst, R. Puzniak, A. Wisniewski, and P. Bordet, Physica C **385**, 42 (2003).

[24] Å. A. F. Olsen, H. Hauglin, T. H. Johansen, P. E. Goa, and D. Shantsev, Physica C **408**, 537 (2004).

[25] M. Cantoni, M. Uchida, Y. Matsui, S. Takekawa, T. Tsuruta, and S. Horiuchi, J. Electron Microsc. **47**, 443 (1998)

[26] C. H. Sow, K. Harada, A. Tonomura, G. Crabtree, and D. G. Grier, Phys. Rev. Lett. **80**, 2693 (1998).

[27] B. Delaunay, Otdelenie Matematicheskikh i Estestvennykh Nauk **7**, 793 (1934).

[28] J. Schindelin, I. Arganda-Carreras, E. Frise, V. Kaynig, M. Longair, T. Pietzsch, S. Preibisch, C. Rueden, S. Saalfeld, B. Schmid, J.-Y. Tinevez, D. J. White, V. Hartenstein, K. Eliceiri, P. Tomancak, and A. Cardona, Nat. Methods **9**, 676 (2012).

[29] W. Meissner and R. Ochsenfeld, Naturwissenschaften **21**, 787 (1933).

[30] J. Auer and H. Ullmaier, Phys. Rev. B **7**, 136 (1973).

[31] P. R. Solomon and Richard E. Harris, Phys. Rev. B **3**, 2969 (1971).